Diffusion and redistribution of lipid-like molecules between membranes in virus-cell and cell-cell fusion systems

Robert J. Rubin and Yi-der Chen
Laboratory of Chemical Physics, National Institute of Diabetes and Digestive and Kidney Diseases, National Institutes of Health, Bethesda, Maryland 20892 USA

ABSTRACT The kinetics of redistribution of lipid-like molecules between the membranes of two fused spherical vesicles is studied by solving the time-dependent diffusion equation of the system. The effects on the probe redistribution rate of pore size at the fusion junction and the relative sizes of the vesicles are examined. It is found that the redistribution rate constant decreases significantly, but not drastically, as the relative size of the pore to that of the vesicles decreases (the bottleneck effect). In general, the time scale of the probe redistribution rate is determined by the size of the vesicle that is loaded with the probe before the activation of the fusion. For a pore size 50 Å in diameter and a typical diffusion coefficient of 10^{-8} cm^2/s for lipids, the mixing half times for typical virus-cell and cell-cell fusion systems are <30 ms and above 200 s, respectively. Thus, although the redistribution of lipid-like probes by diffusion is not rate limiting in virus-cell fusion, redistribution by diffusion is close to rate limiting in spike-protein mediated cell-cell fusion.

1. INTRODUCTION

Recently fluorescent lipid-like R-18 (octadecyl rhodamine B chloride) molecules have been used extensively in monitoring the kinetics of activation reactions of fusion of cells with enveloped viruses or with hemagglutinin-expressed cells (1–7). The principle of the method relies upon the self-quenching properties of this dye: the intensity of total fluorescence decreases when the density of the dye increases and vice versa. Thus, upon fusing of R-18 containing membranes with membranes devoid of the probe, the surface density of the dye decreases because of dye redistribution, resulting in an increase in the total fluorescence. As a result, kinetic properties of fusion can be studied by measuring the rate of fluorescence dequenching.

In general, the macroscopic dequenching signals of a fusion system contain two kinetic components: (*a*) the fusion activation reactions leading to the opening of pore(s) and the coalescing of the membranes; (*b*) the redistribution or mixing of the probes between the coalesced membranes. It is only when the probe redistribution is not rate-limiting that the dequenching data accurately reflects the kinetics of fusion activation reactions (8). So far as we are aware, probe mixing is always assumed to be fast (not rate limiting); and the dequenching kinetics has been used directly in the elucidation of fusion activation mechanisms (4–7). The correctness of this assumption has never been examined.

If R-18 molecules diffuse like lipids with a diffusion coefficient of 10^{-8} cm^2/s, the half time to escape an area of the size of a virus (0.1 μm in diameter) on a plane is in the order of milliseconds. The half time of a typical R-18 dequenching curve in virus-cell fusion systems is in the order of seconds (4–6). Thus, it seems reasonable to assume that R-18 redistribution is not rate limiting. However, recent video microscopic measurements on single virus-cell fusion complexes (9, 10) have shown that the redistribution half time of R-18 molecules is in the "seconds," rather than the "milliseconds," time domain. These findings not only invalidate the fast probe-redistribution assumption, but also raise a question about the nature or cause of this slow redistribution.

In the early stage of fusion, the junction between the two fused vesicles is very small and could form a bottleneck for diffusion (see Fig. 1). It is natural to ask whether this bottleneck is the cause of slow probe redistribution. To resolve this question, we examine in this paper the effect of the size of the bottleneck on the diffusion of lipid-like molecules in a fused complex by solving the time-dependent diffusion equation of the system. We find that the size of the bottleneck does have a significant effect on the redistribution rate. But in the virus-cell fusion case, the bottleneck effect alone is not sufficient to increase the redistribution half time from milliseconds to seconds. On the other hand, the half time for redistribution of lipid-like molecules in the spike-protein expressed cell-cell fusion case is found to be in the order of seconds, similar to that found in dequenching kinetic measurements (6, 7).

In the next section, we briefly describe the coupled partial differential equations for the diffusion of particles on the surface of a fusion complex and present the final

0006-3495/90/11/1157/11 $2.00

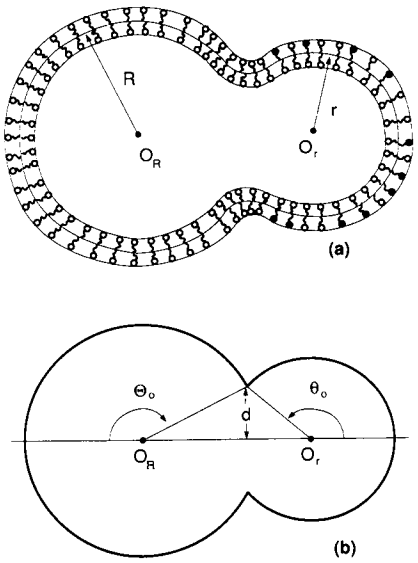

FIGURE 1 (*a*) Schematic drawing of a fusion complex. The lipid-like probes, shown as molecules with filled heads, are initially loaded to the *r*-vesicle only. The radii, *r* and *R*, are measured from the centers of the vesicles to the middle of the bilayer membrane. (*b*) The redistribution of probes in a fusion complex as shown in *a* is modeled as a diffusion of massless particles on the surface of two coalesced spheres. The size of the bottleneck is denoted by *d*.

solution of the equations. The details of the derivation of the solution are given in Appendix A. In section 3, the results obtained are then applied to the calculation of probe redistribution kinetics in representative virus-cell and cell-cell fusion systems, focusing on the effect of the size of the bottleneck at the fusion junction.

2. THE MODEL AND THE DIFFUSION EQUATIONS

A fusion complex composed of two coalesced lipid bilayer vesicles is shown schematically in Fig. 1 *a*. Probe molecules are loaded only on the outer layer of one bilayer vesicle; and at time $t = 0$ start to diffuse to the other vesicle bilayer through the junction (the bottleneck). We evaluate the rate of redistribution of probes as a function of time for different relative dimensions of the bottleneck and cell (or virus).

We neglect the nonzero size of the probe molecules and treat their redistribution as a continuum diffusion process. The problem under investigation involves the diffusion of particles constrained to lie in the surface bilayer of the portions of two coalesced spherical vesicles as shown in Fig. 1 *b*, where the radii *r* and *R* refer to the distances between the center of a vesicle and the mid-point of its bilayer and the radius of the bottleneck is denoted by *d*. It is easy to see from Figs. 1, *a* and *b* that the smallest value of *d* is one-half of the thickness of the bilayer membrane. It follows from the axial symmetry of the coalesced structure and the initial surface density that the time-dependent density of probes is a function of only one polar angle on each vesicle, either θ or Θ. Let $n(\theta, t)$ and $N(\Theta, t)$ be the surface densities of probes on the *r*-sphere and *R*-sphere, respectively. Then each density obeys a diffusion equation:

$$\frac{\partial n}{\partial t} = \frac{D}{r^2}\frac{1}{\sin\theta}\frac{\partial}{\partial\theta}\left(\sin\theta\frac{\partial n}{\partial\theta}\right), \quad 0 \le \theta \le \theta_0 \tag{1}$$

and

$$\frac{\partial N}{\partial t} = \frac{\mathcal{D}}{R^2}\frac{1}{\sin\Theta}\frac{\partial}{\partial\Theta}\left(\sin\Theta\frac{\partial N}{\partial\Theta}\right), \quad 0 \le \Theta \le \Theta_0, \tag{2}$$

where D and $\mathcal{D}$ are the diffusion coefficients of probes in the vesicle bilayers. The surface densities on the two partial spheres are related to one another at the junction, or bottleneck, between them by two continuity laws: (*a*) continuity of surface density

$$n(\theta_0, t) = N(\Theta_0, t); \tag{3}$$

and (*b*) continuity of diffusive flux

$$\frac{D}{r}\frac{\partial n}{\partial\theta}\bigg|_{\theta=\theta_0} = -\frac{\mathcal{D}}{R}\frac{\partial N}{\partial\Theta}\bigg|_{\Theta=\Theta_0} \tag{4}$$

The minus sign in Eq. 4 is required because both angle variables, θ and Θ, shown in Fig. 1 *b* increase toward the junction. The angles θ_0 and Θ_0 are the two maximum polar angles determined by the size of the bottleneck (see Fig. 1 *b*). That is, $d = r\sin\theta_0 = R\sin\Theta_0$.

The system of Eqs. 1–4 are to be solved for the initial condition

$$n(\theta, 0) = n_0, \quad 0 \le \theta \le \theta_0 \tag{5}$$

and

$$N(\Theta, 0) = 0, \quad 0 \le \Theta < \Theta_0, \tag{6}$$

where n_0 is the initial uniform surface density of probes on the *r*-sphere.

The problem of solving a single diffusion equation such as Eq. 1 or 2 on a restricted portion of a sphere has arisen in physical chemical studies in condensed media. For example, in the case of restricted motion of a molecule with cylindrical symmetry, the cylinder axis could be confined to move within a conical volume. Such molecular rotational motion, unrestricted or restricted, is usually

described in terms of diffusional motion of the projection of the axis of the molecule on the unit sphere. This diffusion-in-a-cone model was first formulated by Warchol and Vaughn (11) to treat dielectric relaxation of molecules in glassy matrices and later extended by Wang and Pecora (12) to treat time-correlation functions in light scattering and fluorescence depolarization experiments. Any of the classical methods for solving the diffusion-in-a-cone initial value problem can be generalized to solve the initial value problem treated in this paper, Eq. 1–6, by requiring that the solutions for each partial sphere must join smoothly (satisfy Eqs. 3 and 4). Details of the method of solution are outlined in Appendix A. The final expressions for $n(\theta, t)$ and $N(\Theta, t)$ are obtained as

$$n_0^{-1} n(\theta, t) = \frac{A_r}{A_r + A_R} + \sum_{n=1}^{\infty} h_n \exp\left[\sigma_n \frac{(D\mathcal{D})^{1/2}}{rR} t\right] \cdot {}_2F_1\left[a(\sigma_n), 1 - a(\sigma_n); 1; \frac{1 - \cos\theta}{2}\right] \quad (7)$$

and

$$n_0^{-1} N(\Theta, t) = \frac{A_r}{A_r + A_R} + \sum_{n=1}^{\infty} H_n \exp\left[\sigma_n \frac{(D\mathcal{D})^{1/2}}{rR} t\right] \cdot {}_2F_1\left[A(\sigma_n), 1 - A(\sigma_n); 1; \frac{1 - \cos\Theta}{2}\right], \quad (8)$$

where ${}_2F_1$ [. . .] is an associated Legendre function expressed as a hypergeometric function (11–13) and A_r and A_R are the surface areas of the partial spheres

$$A_r = 2\pi r^2 (1 - \cos\theta_0) \quad (9)$$

and

$$A_R = 2\pi R^2 (1 - \cos\Theta_0). \quad (10)$$

The σ_n's in Eqs. 7 and 8 are the zeros of the function

$$\mathcal{F}(\sigma, z_0, Z_0) = {}_2F_1[a, 1 - a; 1; z_0] + \left(\frac{{}_2F_1[1 + a, 2 - a; 2; z_0]}{{}_2F_1[1 + A, 2 - A; 2; Z_0]}\right) {}_2F_1[A, 1 - A; 1; Z_0], \quad (11)$$

where z_0 and Z_0 are defined, respectively, in Eqs. A7′ and A8′ of Appendix A. The definitions of $a(\sigma)$, $A(\sigma)$, and h_n are given in Eqs. A-14, A-15, and A-29, respectively. It is readily seen in Eqs. 7 and 8 that the surface density on each sphere approaches, at large values of the time, the initial surface density diluted by the area fraction, $A_r(A_r + A_R)^{-1}$.

The rate of redistribution of probes on a fusion complex is usually characterized by a quantity defined as the fraction of the initial amount of probes on the r-sphere which is in excess of the final amount:

$$\eta(t) = [\rho(t) - \rho(\infty)]/[\rho(0) - \rho(\infty)] = \left(1 + \frac{A_r}{A_R}\right) \sum_{n=1}^{\infty} h_n \exp\left[\sigma_n \frac{(D\mathcal{D})^{1/2}}{rR} t\right] \cdot {}_2F_1\left[a(\sigma_n), 1 - a(\sigma_n); 2; \frac{1 \cos\theta_0}{2}\right], \quad (12)$$

where $\rho(t)$ is the fraction of probes which remain on the r-sphere at time t and can be obtained from Eq. 7 as (see Appendix A)

$$\rho(t) = \frac{A_r}{A_r + A_R} + \sum_{n=1}^{\infty} h_n \exp\left[\sigma_n \frac{(D\mathcal{D})^{1/2}}{rR} t\right] \cdot {}_2F_1\left[a(\sigma_n), 1 - a(\sigma_n); 2; \frac{1 - \cos\theta_0}{2}\right]. \quad (13)$$

3. ILLUSTRATIVE CALCULATIONS

As described in the preceding section, the rate of probe redistribution in a fusion complex depends on five parameters: the sizes of the fusing vesicles, r and R; the size of the bottleneck at the junction, d; and the diffusion coefficients of probes on the two vesicles, D and $\mathcal{D}$. Rather than explore the whole parameter space, we will examine the effect of two relative length scales on the redistribution rate of probes: (*a*) the relative size of the bottleneck to that of a vesicle; and (*b*) the relative size of the two fusing vesicles. The first effect deals with the question of whether the existence of a bottleneck will drastically slow down the redistribution rate and the second one concerns the difference in redistribution half times between typical virus-cell and cell-cell fusion systems.

The main step in the calculation of $n(\theta, t)$, and therefore $\rho(t)$ and $\eta(t)$ involves the evaluation of the roots of Eq. 11 and the values of the slope of $\mathcal{F}$ at these roots (see Eq. A-29). All the calculations were done with the Cray supercomputer of the National Cancer Institute at the Frederick campus of National Institutes of Health. For simplicity, we have set $D = 1\ \mu^2/s$ (or 10^{-8} cm^2/s). The results for a few typical cases are shown in Fig. 2 in which the value of the excess fraction, $\eta(t)$ in Eq. 12, is plotted as a function of the dimensionless time, Dt/R^2. As shown by the dashed curves in Fig. 2 *A*, decreasing the relative size of the bottleneck, d/r, at a constant r/R ratio ($r/R = 0.35$) increases the redistribution time (from curve *a* to *c*). However, although it is significant, the increase in redistribution time due to the decrease in d/r is not drastic. For example, whereas the decrease in d from curve *a* to *c* is ~100-fold (from 0.1 to 0.0014), the increase in half time ($t_{1/2}$) is only ~2 (from 0.85 to 1.95).

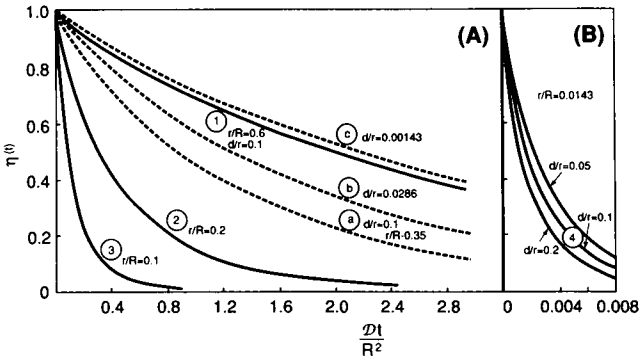

FIGURE 2 The $\eta(t)$, the fraction of the initial amount of probes on the r-sphere which is in excess of the final amount, is plotted as a function of the dimensionless quantity, $\mathcal{D}t/R^2$, for a number of cases showing the effect of the bottleneck size and the effect of relative sizes of the two vesicles. The effect of the bottleneck size on the kinetics of redistribution is shown by the three dashed curves in A for cell-cell fusion systems and the three solid curves in B for virus-cell fusion systems. The four solid curves labeled 1–4 in A and B show the effect of r on the rate of redistribution at constant R and d/r.

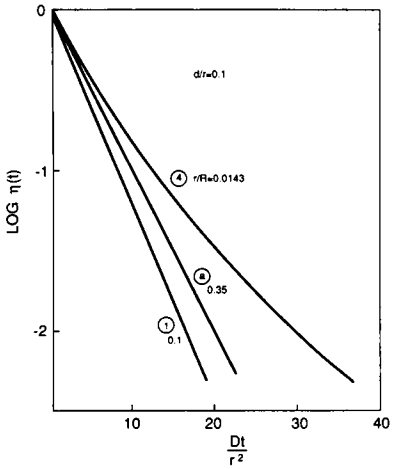

FIGURE 3 The curves labeled as 1, 4, and a in Fig. 2 are replotted as a function of the dimensionless quantity, Dt/r^2. This plot shows the effect of R on the rate of redistribution at constant r and d/r. The use of a semi-log plot here is to show where $\eta(t)$ can be approximated as a single exponential function of the time.

Using these three curves, we have found that the redistribution half time for this case is approximately proportional to the inverse one-fourth power of the radius of the bottleneck. The exact relation between $t_{1/2}$ and d in the limit $d \rightarrow 0$ is discussed in Appendix B. One must note that the r/R value used in these curves (0.35) is approximately equal to the ratio of the radii of red blood cell (RBC) and GP4F cell. As shown in Fig. 2 B, a similar result is obtained for a smaller r/R ratio (0.0143) corresponding roughly to the case of a virus and a red blood cell.

The solid curves labeled 1 to 4 in Figs. 2, A and B illustrate the effect of relative vesicle sizes on the kinetics of probe redistribution. From these curves, one can see that for fixed R the redistribution half time decreases when the radius of the vesicle containing the probes (the r-sphere) becomes smaller. This is not surprising because the time for a probe to diffuse out of the r-sphere becomes shorter when the dimension of the sphere diminishes. Approximately, the redistribution half time is proportional to the second power of r (or r/R). In Fig. 3, three of the curves with varying r/R, but constant d/r, are plotted (semilogarithmically) as a function of the dimensionless time, Dt/r^2. From this plot the effect of R on the redistribution rate at constant r (and d/r) can be assessed. As can be seen from the figure, $t_{1/2}$ increases slightly when R is increased from $1.67r$ to $70r$. That is, the rate of probe redistribution is not very sensitive to the size of the receiving vesicle. In other words, the time scale of probe redistribution kinetics in membrane fusion is largely determined by the size of the r-sphere.

Another interesting result one can see easily from Figs. 2 and 3 is that $\eta(t)$ decays as a single exponential in t when r/R is close to 1 and as a sum of many exponentials when r/R is small. That is, the rate of redistribution of lipid-like probes in cell-cell fusion systems can be expressed approximately with one single exponential, while more than one exponential has to be retained when r/R is much smaller than 1 as in typical virus-cell fusion systems. This point is shown graphically in Figs. 4 and 5, where the amplitude (the coefficient) of each exponential term in Eq. 13 is plotted as a function of the root index n for the two cases. As can be seen in Fig. 4, the distribution of the amplitudes is sharply centered at the first root when r/R is very close to 1 and becomes broader as the value of r/R becomes smaller. As the ratio is reduced further to that of the typical virus-cell value, the distribution becomes very broad and the maximum occurs around the 19th root as shown in Fig. 5.

4. DISCUSSION AND CONCLUSIONS

The main purpose of this study was to examine the effect of the bottleneck of a fusion complex on the kinetics of mixing or redistribution of lipid-like molecules between the membranes of the two fused vesicles in virus-cell or cell-cell fusion systems. To this end, the differential equations describing the diffusion of particles on the surface of two coalesced spheres were formulated and numerical procedures for the solution of these equations

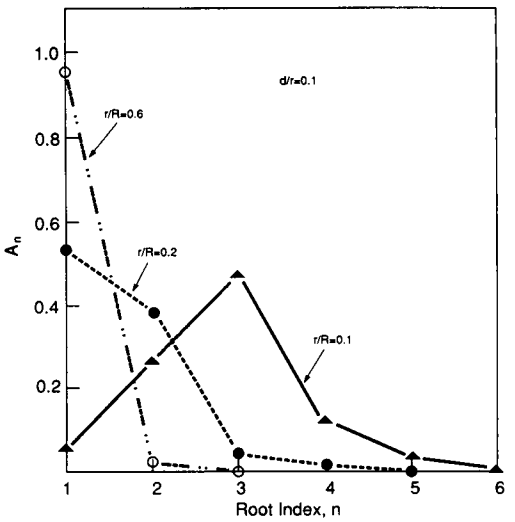

FIGURE 4 The distribution of the contribution (or the amplitude) of each exponential term in Eq. 13 as a function of r/R. The distribution is sharply centered at the first term ($n = 1$) for r/R close to unity and shifts to larger n when r/R is decreased.

were developed. From the results of a few illustrative calculations, a number of interesting general conclusions were obtained in parameter ranges of interest in virus-cell or cell-cell fusion studies. (*a*) Although diffusion is retarded by the bottleneck, the reduction in the redistribution rate is not sensitive to the size of the bottleneck. We find that the mixing half time of particles between the two fused membranes is approximately proportional to the inverse one-fourth power of the radius of the bottleneck. (*b*) The time scale of the probe redistribution rate based on diffusion is mainly determined by the dimension of the *r*-sphere where the probe is initially loaded. Thus, for the same r value, the redistribution half time is almost independent of the size of the R-sphere. On the other hand, for the same R, the half time is approximately proportional to the second power of the value of r. (c) When the sizes of the two fusing vesicles are comparable, the kinetics of redistribution can be described by a single exponential function. In contrast, the redistribution kinetics becomes multi-exponential if the sizes of the two vesicles are quite different.

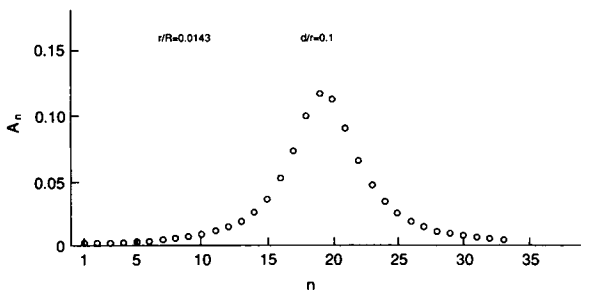

FIGURE 5 The distribution of the amplitudes for the virus-cell fusion case.

In Fig. 2 *B*, the kinetics of probe redistribution for the fusion of influenza virus ($r = 0.05\ \mu$) and red blood cell ($R = 3.5\ \mu$) is obtained for three bottleneck sizes. The redistribution half times estimated from Fig. 2 *B* are tabulated in Table 1. As shown in the table, if the diffusion coefficient is taken at 10^{-8} cm^2/s, a typical value for lipids in cell membranes, in both the virus and the red blood cell membranes, the redistribution half time is ~26 ms for a bottleneck of $d = 25$ Å and decreases to ~14 ms when d is increased to 100 Å. Because the thickness of a typical cell membrane is ~50 Å, the smallest value of d that a fusion complex can have is ~25 Å (see Fig. 1). Thus, 26 ms seems to be the upper bound of the redistribution half time in influenza virus-RBC fusion. This value is quite different, smaller by several orders of magnitude, from what has been measured experimentally on the influenza virus-red blood cell fusion system using R-18 molecules and video microscopy (9, 10). This indicates that the transport of R-18 molecule from the virus membrane to the red blood cell membrane might involve a more complex mechanism than the simple diffusion mechanism modeled in Eqs. 1–4. Either the existence of a diffusion barrier at the bottleneck or a tight binding of R-18 to immobile molecules may have to be invoked to explain the slow rate of R-18 redistribution in this system.

If the radii of RBC and GP4F cells are taken as 3.5 and 10 μm, respectively, the mixing half time of R-18 in fusion of these two cells can be estimated from the curves *a–c* in Fig. 2 *A*. The results are also shown in Table 1. It is found that the half time for $d = 50$ Å is ~200 s. Even when the bottleneck is as large as 1,000 Å, the half time is still

TABLE 1 The redistribution half time for lipid-like probes as a function of the bottleneck size*

r	R	r/R	d	d/r	$t_{1/2}$	$\tau_{1/2}^{\ddagger}$
μ	μ		μ		s	$s^{\ddagger}$
3.5	10	0.35	0.005	0.00143	215	215
—	—	—	0.1	0.0286	125	90
—	—	—	0.35	0.1	87	63
0.05	3.5	0.0143	0.0025	0.05	0.026	
—	—	—	0.005	0.1	0.02	
—	—	—	0.01	0.2	0.014	

*The diffusion coefficient is taken as 1 μ^2/s.
‡This half-time is calculated based on the analytic one-term exponential expression discussed in Appendix B.

larger than 100 s. These results suggest that in the virus glycoprotein-expressed cell-cell fusion between RBC and GP4F cells the fluorescence dequenching signal measured in cuvette experiments (6, 7) might not be used directly to evaluate the kinetics of fusion activation reactions because the R-18 redistribution reaction might be rate limiting. In this case, the procedures presented in reference 8 may have to be used to extract information on fusion activation from macroscopic dequenching data.

We would like to emphasize that the $\eta(t)$ and $\rho(t)$ in Eqs. 12 and 13 can be directly used to interpret the kinetics of fluorescence change on the r-sphere if the fluorescent probes are not self-quenching. In fact, these two equations are directly applicable to any probe as long as the signal of the probe is a linear function of the probe concentration. For self-quenching fluorescent probes (such as R-18 molecules), Eqs. 12 and 13 are no longer usable due to the nonlinear relationship between fluorescence intensity and probe concentration. In this case, the time-dependent surface density function in Eq. 7 (or 8) can be used to calculate the fluorescence kinetics. Recently, spatial fluorescence intensities of R-18 as a function of time have been observed in single RBC-GP4F fusion complexes (6, 7). A detailed analysis of these spatial fluorescence patterns using the formulae developed in this paper should yield more information about the mechanisms of probe (R-18) redistribution on the surface of a fusion complex. This will be the subject of another paper.

Finally, we mention that, in case the pore at the fusion junction is very small compared with the radii of the two fusing vesicles, the analytic solutions of the diffusion problem obtained in this paper can be greatly simplified (see Appendix B). In addition to providing a check on the correctness of the numerical procedures presented in this paper, these approximate analytic expressions are also very useful in discussing related aspects of this diffusion problem, such as the dependence of the half time for redistribution on the various length parameters (see values of $\tau_{1/2}$ in the last colum in Table 1 calculated from Eqs. B22 and B23), the estimate of the approximate zeros (σ_n) of $\mathcal{F}$ in Eqs. 11 and 12, the extension of the problem to related one- and three-dimensional systems, etc. The results of these analyses will be reported in a separate paper.

In conclusion, we have developed a numerical procedure for the calculation of diffusion of molecules on the surface of two coalesced spheres. The procedure is new and is useful in studying the rate of redistribution of lipid-like probes in virus-cell or cell-cell fusion systems. The formulae derived can be used directly to deduce the change of fluorescence (or other signals) due to the redistribution of the probes.

APPENDIX A

Formal solution of probe redistribution problem

In this appendix, we outline the Laplace transform method (14), which we have used to determine explicit expressions for the solutions of Eqs. 1–4 with the initial conditions Eqs. 5 and 6. The Laplace transforms of Eqs. 1–4 are

$$\frac{D}{r^2}\frac{1}{\sin\theta}\frac{d}{d\theta}\left(\sin\theta\frac{d\tilde{n}}{d\theta}\right) = p\tilde{n} - n_0, \quad 0 \le \theta \le \theta_0 \tag{A1}$$

and

$$\frac{\mathcal{D}}{R^2}\frac{1}{\sin\Theta}\frac{d}{d\Theta}\left(\sin\Theta\frac{d\tilde{N}}{d\Theta}\right) = p\tilde{N}, \quad 0 \le \Theta \le \Theta_0 \tag{A2}$$

$$\tilde{n}(\theta_0, p) = \tilde{N}(\Theta_0, p) \tag{A3}$$

and

$$\frac{D}{r}\frac{d\tilde{n}}{d\theta}\bigg|_{\theta=\theta_0} = -\frac{\mathcal{D}}{R}\frac{d\tilde{N}}{d\Theta}\bigg|_{\Theta=\Theta_0}, \tag{A4}$$

where a tilde superscript on the surface density variables n and N denotes the Laplace transform of the variable,

$$\tilde{n}(\theta, p) = \int_0^\infty dt\, e^{-pt}\, n(\theta, t) \tag{A5}$$

and

$$\tilde{N}(\Theta, p) = \int_0^\infty dt\, e^{-pt}\, N(\Theta, t). \tag{A6}$$

It is convenient to introduce new independent variables

$$z = \tfrac{1}{2}(1 - \cos\theta) \tag{A7}$$

and

$$Z = \tfrac{1}{2}(1 - \cos\Theta) \tag{A8}$$

in Eqs. A1–A4 and two new parameters

$$\sigma = \frac{rR}{(D\mathcal{D})^{1/2}}p \tag{A9}$$

and

$$\epsilon = \frac{r}{R}\left(\frac{\mathcal{D}}{D}\right)^{1/2}. \tag{A10}$$

The new set of equations is

$$z(1-z)\frac{d^2\tilde{n}}{dz^2} - (1-2z)\frac{d\tilde{n}}{dz} - \epsilon\sigma\tilde{n} = -n_0\frac{r^2}{D}, \quad 0 \le z \le z_0 < 1 \tag{A1'}$$

$$Z(1-Z)\frac{d^2\tilde{N}}{dZ^2}-(1-2Z)\frac{d\tilde{N}}{dZ}-\frac{1}{\epsilon}\sigma\tilde{N}=0,$$

$$0\le Z\le Z_0<1 \quad (A2')$$

$$\tilde{n}(z_0,\sigma)=\tilde{N}(Z_0,\sigma) \quad (A3')$$

and

$$-\frac{D}{r^2}\frac{d\tilde{n}}{dz}\bigg|_{z=z_0}=\frac{\mathcal{D}}{R^2}\frac{d\tilde{N}}{dZ}\bigg|_{Z=Z_0}, \quad (A4')$$

where

$$z_0=\tfrac{1}{2}(1-\cos\theta_0) \quad (A7')$$

$$Z_0=\tfrac{1}{2}(1-\cos\Theta_0) \quad (A8')$$

and we have used the relation (see Fig. 1 *b*)

$$r\sin\theta_0=R\sin\Theta_0 \quad (A11)$$

in obtaining Eq. A4'.

The most general regular solutions of the pair of ordinary differential Eqs. A1' and A2' are

$$\tilde{n}(z,\sigma)=\frac{n_0r^2}{\epsilon D\sigma}+c_r{}_2F_1[a,1-a;1;z] \quad (A12)$$

and

$$\tilde{N}(Z,\sigma)=c_R{}_2F_1[A,1-A;1;Z], \quad (A13)$$

where

$$a=\tfrac{1}{2}-\tfrac{1}{2}[1-4\epsilon\sigma]^{1/2}, \quad (A14)$$

$$A=\tfrac{1}{2}-\tfrac{1}{2}[1-4\sigma/\epsilon]^{1/2}, \quad (A15)$$

and the hypergeometric function has the convergent expansion

$${}_2F_1[b,c;d;z]=\sum_{n=0}^{\infty}\frac{(b)_n(c)_n}{(d)_n(1)_n}z^n, \quad |z|<1. \quad (A16)$$

The symbol $(e)_n$ in Eq. A16 denotes a product of n factors

$$(e)_n=e(e+1)(e+2)\cdots(e+n-1) \quad (A17)$$

with the convention that $(e)_0=1$. The integration constants, c_r and c_R, are determined by requiring that the solutions Eqs. A12 and A13 join smoothly at the bottleneck junction, Eqs. A3' and A4'. Substituting Eqs. A12 and A13 into Eqs. A3' and A4' yields a pair of simultaneous equations for c_r and c_R whose solution is

$$c_r=-\frac{n_0r^2}{\epsilon D\sigma}\left(\frac{1}{\mathcal{F}(\sigma,z_0,Z_0)}\right) \quad (A18)$$

and

$$c_R=\frac{n_0r^2}{\epsilon D\sigma}\left(\frac{1}{\mathcal{F}(\sigma,z_0,Z_0)}\right)\left(\frac{{}_2F_1[1+a,2-a;2;z_0]}{{}_2F_1[1+A,2-A;2;Z_0]}\right), \quad (A19)$$

where

$$\mathcal{F}(\sigma,z_0,Z_0)={}_2F_1[a,1-a;1;z_0]+\left(\frac{{}_2F_1[1+a,2-a;2;z_0]}{{}_2F_1[1+A,2-A;2;Z_0]}\right){}_2F_1[A,1-A;1;Z_0]. \quad (A20)$$

The expressions for c_r and c_R have been simplified with the aid of the relations

$$\frac{d}{dz}{}_2F_1[b,c;d;z]=\frac{bc}{d}{}_2F_1[1+b,1+c;1+d;z], \quad (A21)$$

$$a(1-a)=\epsilon\sigma, \quad (A22)$$

and

$$A(1-A)=\frac{\sigma}{\epsilon}. \quad (A23)$$

The final expressions for the solutions of Eqs. A1' and A2', the Laplace transforms, $\tilde{n}(z,\sigma)$ and $\tilde{N}(Z,\sigma)$, are

$$\tilde{n}(z,\sigma)=\frac{n_0r^2}{\epsilon D}\frac{1}{\sigma}\left\{1-\frac{{}_2F_1[a,1-a;1;z]}{\mathcal{F}(\sigma,z_0,Z_0)}\right\} \quad (A24)$$

and

$$\tilde{N}(Z,\sigma)=\frac{n_0r^2}{\epsilon D}\frac{1}{\sigma}\cdot\left\{\frac{{}_2F_1[A,1-A;1;Z_0]}{\mathcal{F}(\sigma,z_0,Z_0)}\left(\frac{{}_2F_1[1+a,2-a;2;z_0]}{{}_2F_1[1+A,2-A;2;Z_0]}\right)\right\}. \quad (A25)$$

Having derived explicit expressions for the Laplace transforms of the surface densities in Eqs. A24 and A25, the inversion theorem for the Laplace transformation (14) can be used to obtain explicit expressions for the corresponding time-dependent quantities, e.g.,

$$n(\theta,t)=\frac{1}{2\pi i}\int_{c-i\infty}^{c+i\infty}dp\,e^{pt}\,\tilde{n}(\theta,p) \quad (A26)$$

or

$$n(z,t)=\frac{1}{2\pi i}\int_{c-i\infty}^{c+i\infty}d\sigma\exp\left\{\sigma\frac{(D\mathcal{D})^{1/2}}{rR}t\right\}\cdot\frac{n_0}{\sigma}\left\{1-\frac{{}_2F_1[a,1-a;1;z]}{\mathcal{F}(\sigma,z_0,Z_0)}\right\}, \quad (A27)$$

where the path of integration lies to the right of all singularities of $\tilde{n}(z,\sigma)$. The integrand in Eq. A27 has simple poles at $\sigma=0$ and also at the simple zeros $\sigma=\sigma_n$, $n=1,2,\ldots$ of $\mathcal{F}(\sigma,z_0,Z_0)$ which, as we will see in what follows, lie on the negative real σ-axis. Therefore, it follows from the theory of residues (14, 15) that the contour integral Eq. A27 reduces to a sum of residues of the integrand at these poles

$$n(z,t)=n_0\left\{1-\frac{1}{1+\left(\frac{1-Z_0}{1-z_0}\right)}+\sum_{n=1}^{\infty}h_n{}_2F_1[a(\sigma_n),1-a(\sigma_n);1;z]\exp\left(\sigma_n\frac{(D\mathcal{D})^{1/2}}{rR}t\right)\right\}, \quad (A28)$$

where

$$h_n = -\left(\sigma_n \frac{d}{d\sigma}\{\mathcal{F}(\sigma, z_0, Z_0)\}\Big|_{\sigma=\sigma_n}\right)^{-1}. \quad \text{(A29)}$$

It can easily be shown that the time-independent term on the right-hand side in Eq. A28 reduces to

$$1 - \left(1 + \frac{1 - Z_0}{1 - z_0}\right)^{-1} = \frac{A_r}{A_r + A_R} \quad \text{(A30)}$$

with the aid of the identity at the bottleneck, $r \sin \theta_0 = R \sin \Theta_0$, where A_r and A_R are the areas of the partial spheres, Eqs. 13 and 14.

In addition to the local surface density, Eq. A28, another quantity of interest which characterizes the redistribution of probes is the fraction of the total number of probes remaining on the r-sphere at time t

$$\begin{aligned}\rho(t) &= n_T(t)/n_T(0) \\ &= \frac{2\pi r^2}{n_T(0)} \int_0^{\theta_0} d\theta \sin\theta\, n(z, t) \\ &= \frac{4\pi r^2}{n_T(0)} \int_0^{z_0} dz\, n(z, t), \end{aligned} \quad \text{(A31)}$$

where $n_r(0) = n_0 \cdot A_r$. Substituting Eqs. A28 and A30 in Eq. A31 and using the identity,

$$\int_0^{z_0} dz\, {}_2F_1[a, 1 - a; 1; z] = z_0 {}_2F_1[a, 1 - a; 2; z_0], \quad \text{(A32)}$$

we obtain

$$\rho(t) = \frac{A_r}{A_r + A_R} + \sum_{n=1}^{\infty} h_n {}_2F_1[a(\sigma_n), 1 - a(\sigma_n); 2; z_0] \cdot \exp\left(\sigma_n \frac{(D\mathcal{D})^{1/2}}{rR} t\right). \quad \text{(A33)}$$

Because the initial value of the fraction, $\rho(t)$, is $\rho(0) = 1$, a very useful "sum rule" follows from Eq. A33

$$\left(1 + \frac{A_r}{A_R}\right) \sum_{n=1}^{\infty} h_n {}_2F_1[a(\sigma_n), 1 - a(\sigma_n); 2; z_0] = 1. \quad \text{(A34)}$$

An equivalent alternate form of Eq. A33 which starts at unity and decays to zero, instead of $A_r/(A_r + A_R)$, as t increases is

$$\eta(t) = [\rho(t) - \rho(\infty)]/[\rho(0) - \rho(\infty)] = \left(1 + \frac{A_r}{A_R}\right) \sum_{n=1}^{\infty} h_n \cdot {}_2F_1[a(\sigma_n), 1 - a(\sigma_n); 2; z_0] \exp\left(\sigma_n \frac{(D\mathcal{D})^{1/2}}{rR} t\right). \quad \text{(A35)}$$

Numerical evaluation of $n(\theta, t)/n_0$ or $\eta(t)$ for a particular set of parameters r, R, D, $\mathcal{D}$, and d requires as a first step the determination of the zeros of $\mathcal{F}(\sigma, z_0, Z_0)$ in Eq. A20. The typical diameters of cells and viruses are 5 and 0.1 μ, respectively. With a pore size 0.01 μ in diameter at the fusion junction, the angles θ and Θ_0 are extremely close to π radians (see Fig. 1 *b*, where $\sin\theta_0 = d/r$ and $\sin\Theta_0 = d/R$); and the arguments of the hypergeometric functions in $\mathcal{F}(\sigma, z_0, Z_0)$ are both close to unity. Therefore, the most convenient, or numerically useful, series expansions of the hypergeometric functions in Eq. A20 are their analytic continuations in the vicinity of $z_0 = 1$ and $Z_0 = 1$ (see reference 13, pp 559 and 560, Eqs. 15.3.10 and 15.3.12):

$$\begin{aligned}{}_2F_1[a, 1 - a; 1; z_0] &= \{\Gamma(a)\Gamma(1 - a)\}^{-1} \sum_{n=0}^{\infty} \frac{(a)_n(1 - a)_n}{(1)_n(1)_n} \\ &\cdot [2\psi(n + 1) - \psi(a + n) \\ &- \psi(1 - a + n) - \ln(1 - z_0)](1 - z_0)^n \end{aligned} \quad \text{(A36)}$$

and

$$\begin{aligned}{}_2F_1[1 + a, 2 - a; 2; z_0] &= \{\Gamma(a)\Gamma(1 - a)\}^{-1} \\ &\cdot \left\{\frac{1}{a(1 - a)(1 - z_0)} - \sum_{n=0}^{\infty} \frac{(1 + a)_n(2 - a)_n}{(2)_n(1)_n} \right. \\ &\cdot [\psi(n + 1) + \psi(n + 2) - \psi(1 + a + n) \\ &\left. - \psi(2 - a + n) - \ln(1 - z_0)](1 - z_0)^n\right\}, \end{aligned} \quad \text{(A37)}$$

where the function $\psi(x)$ is the logarithmic derivative of the gamma function (see reference 13, pp 259, Eq. 6.3.1)

$$\psi(x) = \frac{d}{dx} \ln \Gamma(x). \quad \text{(A38)}$$

As mentioned in section 3 of this paper, we have used the Cray supercomputer of the National Cancer Institute to perform the required numerical calculations involving Eqs. A28, A29, A33, A36, and A37.

APPENDIX B

Approximate analytic expression for $\rho(t)$ (and $\eta[t]$)

We will obtain an approximate analytic expression for $\rho(t)$, Eq. A33. In our model of probe redistribution we have assumed that the r-sphere is loaded initially. According to Fig. 1 *b*, where $r \sin\theta_0 = d$,

$$\cos\theta_0 = -(r^2 - d^2)^{1/2}/r, \quad \text{(B1)}$$

and from Eq. A7,

$$z_0 = 1/2 + 1/2\,(1 - d^2/r^2)^{1/2}. \quad \text{(B2)}$$

We are particularly interested in the limit in which both $r \gg d$ and $R \gg d$. In this case, Eq. B2 is approximately

$$z_0 \simeq 1 - (d/2r)^2; \quad \text{(B3)}$$

and there is a similar approximate form for

$$Z_0 \simeq 1 - (d/2R)^2. \quad \text{(B4)}$$

Thus, both $1 - z_0$ and $1 - Z_0$ are very small compared with one in the limiting case of small relative bottleneck size and we need only retain the leading terms in the analytic continuations, Eqs. A36 and A37,

$${}_2F_1[a, 1 - a; 1; z_0] \simeq [\Gamma(a)\Gamma(1 - a)]^{-1} \cdot [2\psi(1) - \psi(a) - \psi(1 - a) - 2\ln(d/2r)] \quad \text{(B5)}$$

and

$$ {}_2F_1[1 + A, 2 - A; 2; Z_0] \simeq [\Gamma(A)\Gamma(1 - A)]^{-1} \frac{1}{A(1 - A)} \left(\frac{2R}{d}\right)^2. \quad \text{(B6)} $$

In the present case, the approximate form for $\mathcal{F}(\sigma, z_0, Z_0)$ in Eq. A20, using one-term approximations such as Eqs. B5 and B6, is

$$ \mathcal{F}(\sigma, z_0, Z_0) \simeq [\Gamma(a)\Gamma(1 - a)]^{-1}\left\{2\psi(1) - \psi(a) - \psi(1 - a) + 2 \ln\left(\frac{2r}{d}\right) + \frac{A(1 - A)}{a(1 - a)}\left(\frac{r^2}{R^2}\right) \cdot \left[2\psi(1) - \psi(A) - \psi(1 - A) + 2 \ln\left(\frac{2R}{d}\right)\right]\right\}. \quad \text{(B7)} $$

Utilizing the definitions of a and A in Eqs. A14 and A15, ϵ in Eq. A10, and the reflection formulas (see reference 13, p 259, Eq. 6.3.7)

$$ \psi(x) = \psi(1 - x) - \pi \cot \pi x, \quad \text{(B8)} $$

and

$$ \Gamma(x)\Gamma(1 - x) = \pi \csc \pi x, \quad \text{(B9)} $$

Eq. B7 for $\mathcal{F}(\sigma, z_0, Z_0)$ reduces to

$$ \mathcal{F}(\sigma, z_0, Z_0) \simeq \pi^{-1} \sin \pi a f(\sigma), \quad \text{(B10)} $$

where

$$ f(\sigma) = 2\psi(1) - 2\psi(1 - a) + \pi \cot \pi a + 2 \ln (2r/d) + (D/\mathcal{D})[2\psi(1) - 2\psi(1 - A) + \pi \cot \pi A + 2 \ln (2R/d)]. \quad \text{(B11)} $$

A second form of $f(\sigma)$ which we will also use is

$$ f(\sigma) = 2\psi(1) + \frac{1}{a} - \psi(1 + a) - \psi(1 - a) + 2 \ln (2r/d) + (D/\mathcal{D})\left[2\psi(1) + \frac{1}{A} - \psi(1 + A) - \psi(1 - A) + 2 \ln (2R/d)\right], \quad \text{(B12)} $$

where Eq. B12 follows from Eq. B7 with the recurrence relation (see reference 13, p 258, Eq. 6.3.5)

$$ \psi(x) = \psi(1 + x) - \frac{1}{x} \quad \text{(B13)} $$

instead of Eq. B8.

There is an analogous one-term approximation for the hypergeometric function (see reference 13, p 559, Eq. 15.3.11), ${}_2F_1[a, 1 - a; 2; z_0]$, in the numerator of the Laplace transform of $\rho(t)$

$$ {}_2F_1(a, 1 - a; 2; z_0] \simeq \pi^{-1} \sin \pi a/\epsilon\sigma. \quad \text{(B14)} $$

Combining the one-term approximations Eqs. B10–B14, we obtain the approximate expression for the Laplace transform of $\rho(t)$,

$$ \tilde{\rho}(\sigma) \simeq \frac{r^2}{\epsilon D} \frac{1}{\sigma}\left[1 - \frac{1}{\epsilon\sigma f(\sigma)}\right]. \quad \text{(B15)} $$

It should be noted that the reason why these one-term approximations provide useful results is related to the fact that the psi-functions, $\psi(a)$ and $\psi(A)$, have simple poles at negative integer values of the arguments, a and A (i.e., on the negative σ-axis). All neglected terms in expansions such as Eqs. A36 and A37 can only have poles where $n + a$ or $n + A$ is a negative integer.

In the remainder of this appendix, we assume that diffusion coefficients are comparable in magnitude and vesicle sizes are comparable in magnitude, i.e., we assume that ϵ is close to unity. In this case, we demonstrate the following three results for $\tilde{\rho}(\sigma)$, Eq. B15, which imply altogether a dominant single exponential relaxation of $\rho(t)$:

(1) There is a small negative root, σ_1, of $\epsilon\sigma f(\sigma) = 0$, where $f(\sigma)$ is given in Eq. B12.

(2) The coefficient of the exponential associated with this root is approximately equal to $A_R/(A_r + A_R)$.

(3) The coefficient of the exponential associated with every root of $\sigma\epsilon f(\sigma) = 0$ is positive. We remark that the proof of this positivity property is not limited to the case $\epsilon \sim 1$.

(1) σ_1 is small in magnitude and negative

To demonstrate that there is a small negative root of $\sigma f(\sigma) = 0$, we will assume that result and then verify it a posteriori. Expand the terms in $\epsilon\sigma f(\sigma)$, Eq. B12, in powers of σ and retain all terms up to the third order in σ. For this purpose, we use the following series expansions:

$$ \epsilon\sigma a^{-1} \simeq 1 - \epsilon\sigma - \epsilon^2\sigma^2 - 2\epsilon^3\sigma^3, \quad \text{(B16)} $$

$$ \epsilon\sigma A^{-1} \simeq \epsilon^2 - \epsilon\sigma - \sigma^2 - 2\epsilon^{-1}\sigma^3, \quad \text{(B17)} $$

$$ A \simeq (\sigma/\epsilon) + (\sigma/\epsilon)^2 + 2(\sigma/\epsilon)^3, \quad \text{(B18)} $$

and

$$ \epsilon\sigma[\psi(1 + a) + \psi(1 - a)] \simeq \epsilon\sigma[2\psi(1) - 2\zeta(3)\epsilon^2\sigma^2], $$
$$ \epsilon\sigma[\psi(1 + A) + \psi(1 - A)] \simeq \epsilon\sigma[2\psi(1) - 2\zeta(3)(\sigma/\epsilon)^2], \quad \text{(B19)} $$

where

$$ \zeta(3) \simeq 1.2021. \quad \text{(B20)} $$

Collecting powers of $\epsilon\sigma$, we arrive at the following cubic equation in $\epsilon\sigma$ which is written in a form suitable for obtaining a solution by iteration:

$$ -\epsilon\sigma = (1 + \epsilon^2 D/\mathcal{D})\{2 \ln (2r/d) - 1 + (D/\mathcal{D})[2 \ln (2R/d) - 1] - \epsilon\sigma(1 + D/\mathcal{D}\epsilon^2) + 2\epsilon^2\sigma^2[\zeta(3) - 1] \cdot (1 + D/\mathcal{D}\epsilon^2)\}^{-1}. \quad \text{(B21)} $$

The zeroth, or starting, approximation for the solution of Eq. B21 is

$$ \epsilon\sigma_1^{(0)} = -(1 + \epsilon^2 D/\mathcal{D})\{2 \ln (2r/d) - 1 + (D/\mathcal{D})[2 \ln (2R/d) - 1]\}^{-1}; \quad \text{(B22)} $$

and the next is

$$\epsilon\sigma_1^{(1)} = \epsilon\sigma_1^{(0)}\left\{1 + [(\epsilon\sigma_1^{(0)})^2 - 2[\zeta(3) - 1](\epsilon\sigma_1^{(0)})^2]\left(\frac{1 + D/\epsilon^2\mathcal{D}}{1 + \epsilon^2 D/\mathcal{D}}\right)\right\}^{-1}. \quad \text{(B23)}$$

It is seen from Eqs. B22 and B23 that if ϵ and $D/\mathcal{D}$ are of order unity, then $\epsilon\sigma_1^{(0)}$ and $\epsilon\sigma_1^{(1)}$ are indeed small as assumed, at least for sufficiently large values of r/d and R/d (as in the case for cell-cell fusion).

(2) The coefficient of the exponential associated with the root $\sigma_1^{(1)}$ (Eq. B23)

The exact time-dependent expression for $\rho(t)$ is given in Eq. A33 with h_n defined in Eq. A29. The approximate time-dependent expression which we obtain in this Appendix in the case of cell-cell fusion is the inverse Laplace transform of $\tilde{\rho}(\sigma)$ in Eq. B15

$$\rho(t) \simeq \frac{1}{2\pi i}\int_{c-i\infty}^{c-i\infty} d\sigma \cdot \exp\left(\sigma\frac{(D\mathcal{D})^{1/2}}{rR}t\right)\frac{1}{\sigma}\left\{1 - \frac{1}{\epsilon\sigma f(\sigma)}\right\}, \quad \text{(B24)}$$

where $f(\sigma)$ is given in Eqs. B11 and B12. However, for σ near $\sigma = 0$, there is the approximate cubic equation related to Eq. B21

$$\epsilon\sigma f(\sigma) \simeq (1 + \epsilon^2 D/\mathcal{D}) + \{2\ln(2r/d) - 1 + (D/\mathcal{D})[2\ln(2R/d) - 1]\}\epsilon\sigma - (1 + D/\epsilon^2\mathcal{D})\epsilon^2\sigma^2 + 2[\zeta(3) - 1](1 + D/\epsilon^2\mathcal{D})\epsilon^3\sigma^3, \quad \epsilon\sigma \ll 1. \quad \text{(B25)}$$

The contour integral Eq. B24 is a sum of residues of the integrand at its poles. We have asserted at the beginning of this Appendix that only the first exponential in the sum of exponentials contributes significantly. We will assume that this is so and verify it subsequently. Thus, we assume that the relaxation of $\rho(t)$ in Eq. B24 is adequately described by the sum of the residues of the integrand in Eq. B24 at $\sigma = 0$ and $\sigma = \sigma_1^{(1)}$. Accordingly, using Eqs. B25 and B23, and the definition of ϵ in Eq. A10, we obtain

$$\rho(t) \simeq 1 - \frac{1}{1 + r^2/R^2} - \exp\left(\sigma_1^{(1)}\frac{(D\mathcal{D})^{1/2}}{rR}t\right) \Big/ \left\{\sigma_1^{(1)}\frac{d}{d\sigma}[\epsilon\sigma f(\sigma)]_{\sigma=\sigma_1^{(1)}}\right\}$$
$$\simeq \frac{r^2}{r^2 + R^2} - \exp\left(\sigma_1^{(1)}\frac{(D\mathcal{D})^{1/2}}{rR}t\right) \Big/ \{[2\ln(2r/d) - 1 + (D/\mathcal{D})\{2\ln(2R/d) - 1\}]\epsilon\sigma_1^{(1)} - 2(1 + D/\epsilon^2\mathcal{D})(\epsilon\sigma_1^{(1)})^2 + 6[\zeta(3) - 1] \cdot (1 + D/\epsilon^2\mathcal{D})(\epsilon\sigma_1^{(1)})^3\} \quad \text{(B26)}$$

$$\simeq \frac{A_r}{A_r + A_R} + \frac{A_R}{A_r + A_R}\exp\left(\sigma_1^{(1)}\frac{(D\mathcal{D})^{1/2}}{rR}t\right) \Big/ \left\{1 + \left(\frac{1 + D/\epsilon^2\mathcal{D}}{1 + \epsilon^2 D/\mathcal{D}}\right)((\epsilon\sigma_1^{(1)})^2 - 4[\zeta(3) - 1](\epsilon\sigma_1^{(1)})^3)\right\}. \quad \text{(B27)}$$

In transforming the denominator to arrive at Eq. B27 from Eq. B26, we have assumed that $\sigma_1^{(1)}$ is the exact root of $\epsilon\sigma_1^{(1)} f(\sigma_1^{(1)}) = 0$ where $\epsilon\sigma f(\sigma)$ is given in Eq. B25; and we have replaced the first-order term in $\epsilon\sigma_1^{(1)}$ by the negative of the zeroth-, second-, and third-order terms. Another relation which is used above,

$$r^2/(r^2 + R^2) \simeq A_r/(A_r + A_R),$$

is obviously valid in the present case where $r \gg d$, $R \gg d$. The exact value of $\rho(t)$ at $t = 0$ is $\rho(0) = 1$; and the approximate value of $\rho(0)$ from Eq. B27 can be written as

$$\rho(0) \simeq 1 - \frac{A_R}{A_r + A_R}\frac{\alpha[\epsilon\sigma_1^{(1)}]^2}{1 + \alpha[\epsilon\sigma_1^{(1)}]^2}, \quad \text{(B28)}$$

where

$$\alpha = \{1 - 4[\zeta(3) - 1](\epsilon\sigma_1^{(1)})\}\left(\frac{1 + D/\epsilon^2\mathcal{D}}{1 + \epsilon^2 D/\mathcal{D}}\right). \quad \text{(B29)}$$

The second term in Eq. B28 is negligible if $[\epsilon\sigma_1^{(1)}]^2$ is negligible. Thus, if we can show that each of the residues at the other poles of $\tilde{\rho}(\sigma)$, Eqs. B15 and B24, is positive, we will have completed our program.

(3) The residue of the integrand at each nonzero pole of $1/f(\sigma)$ adds a positive contribution to $\rho(t)$ (Eq. B24)

We have already shown in Eq. B27 that the contribution of the residue at $\sigma_1^{(1)}$ of the integrand in Eq. B24 is intrinsically positive. To demonstrate this positivity property at the other nonzero poles of $1/f(\sigma)$, we use the expression (Eq. B11) for $f(\sigma)$. If σ_n is such a pole (i.e., $f(\sigma_n) = 0$, $\sigma_n \neq 0$), then the contribution of the residue of the integrand at σ_n to $\rho(t)$ in Eq. B24 is

$$R_n(t) = -\frac{1}{\epsilon\sigma_n^2}\exp\left(\sigma_n\frac{(D\mathcal{D})^{1/2}}{rR}t\right) \Big/ \left\{\frac{d}{d\sigma}f(\sigma)\right\}\Big|_{\sigma=\sigma_n} \quad \text{(B30)}$$

The derivative in the denominator of Eq. B30, based on Eq. B11 for $f(\sigma)$, is

$$\frac{d}{d\sigma}f(\sigma) = -\epsilon(1 - 4\epsilon\sigma)^{-1/2}[\pi^2\csc^2\pi a - 2\psi^1(1 - a)] - (D/\epsilon\mathcal{D})(1 - 4\sigma/\epsilon)^{-1/2}[\pi^2\csc^2\pi A - 2\psi^1(1 - A)], \quad \text{(B31)}$$

where $\psi^1(x)$ denotes $[(d/dx)\,\psi(x)]$, and has the integral representation (see reference 13, p 259, Eq. 6.3.21)

$$\psi^1(x) = \int_0^\infty dt\left(\frac{te^{-xt}}{1 - e^{-t}}\right). \quad \text{(B32)}$$

According to the definitions of a and A in Eqs. A14 and A15, both $1 - a$ and $1 - A$ are ≥ 1 if $\sigma \leq 0$. It follows from Eq. B32 that all values on the

negative σ-axis of $2\psi^1(1 - a)$ and $2\psi^1(1 - A)$ in Eq. B31 are less than or equal to (see reference 13, p 260, Eq. 6.4.2)

$$2\psi^1(1) = \pi^2/3.$$

Because all values of $\pi^2 \csc^2 \pi x$ are greater than or equal to π^2, the square bracket expressions in Eq. B31 are strictly positive, and therefore the residue $R(t)$ in Eq. B30 is intrinsically positive.

We would like to thank Drs. Robert Blumenthal and R. J. Lowy for valuable discussions. We also want to thank Dr. J. V. Maizel for help in the use of supercomputer at the National Cancer Institute.

Received for publication 5 March 1990 and in final form 25 May 1990.

REFERENCES

1. Hoekstra, D., T. de Boer, K. Klappe, and J. Wilschut. 1984. Fluorescence method for measuring the kinetics of fusion between biological membranes. *Biochemistry.* 23:5675–5681.
2. Hoekstra, D., and K. Klappe. 1986. Use of a fluorescence assay to monitor the kinetics of fusion between erythrocyte ghosts, as induced by Sendai virus. *Biosci. Rep.* 6:953–960.
3. Loyter, A., V. Citovsky, and R. Blumenthal. 1988. The use of fluorescence dequenching methods to follow viral membrane fusion events. *Methods Biochem. Anal.* 33:128–164.
4. Blumenthal, R., A. Bali-Puri, A. Walter, D. Covell, and O. Eidelman. 1987. pH-dependent fusion of vesicular stomatitis virus with vero cells: measurement by dequenching of octadecylrhodamine fluorescence. *J. Biol. Chem.* 262:13614–13619.
5. Puri, A., J. Winick, R. J. Lowy, D. Covell, O. Eidelman, A. Walter, and R. Blumenthal. 1988. Activation of vesicular stomatitis virus fusion with cells by pretreatment at low pH. *J. Biol. Chem.* 263:4749–4753.
6. Sarker, D. P., S. J. Morris, O. Eidelman, J. Zimmerberg, and R. Blumenthal. 1989. Initial stages of influenza hemagglutinin-induced cell fusion monitored simultaneously by two fluorescence events: cytoplasmic continuity and lipid mixing. *J. Cell Biol.* 109:113–122.
7. Morris, S. J., D. P. Sarkar, J. M. White, and R. Blumenthal. 1989. Kinetics of pH-dependent fusion between 3T3 fibroblasts expressing influenza hemagglutinin and red blood cells. *J. Biol. Chem.* 264:3972–3978.
8. Chen, Y., and R. Blumenthal. 1989. On the use of self-quenching fluorophores in the study of membrane fusion kinetics; the effect of slow probe redistribution. *Biophys. Chem.* 34:283–292.
9. Lowy, R. J., D. P. Sarkar, Y. Chen, and R. Blumenthal. 1990. Observation of single influenza virus-cell fusion and measurement by fluorescence video microscopy. *Proc. Natl. Acad. Sci.* 87:1850–1854.
10. Giorgiou, G. N., I. E. G. Morrison, and R. J. Cherry. 1989. Digital fluorescence imaging of fusion of influenza virus with erythrocytes. *Febs. (Fed. Eur. Biochem. Soc.) Lett.* 250:487–492.
11. Warchol, M. P., and W. E. Vaughan. 1978. Dielectric relaxation by restricted rotational diffusion. *Adv. Mol. Relax. Interact. Processes.* 13:317–330.
12. Wang, C. C., and R. Pecora. 1980. Time-correlation function for restricted rotational diffusion. *J. Chem. Phys.* 72:5333–5340.
13. Abramowitz, M., and I. A. Stegun. 1964. Handbook of Mathematical Functions. National Bureau of Standards, Applied Mathematical Series, 55. US Government Printing Office. 1046.
14. Carslaw, H. S., and J. C. Jaeger. 1959. Conduction of Heat in Solids. 2nd ed. Clarendon Press, Oxford. 297–352.
15. Whittaker, E. T., and G. N. Watson. 1947. A Course of Modern Analysis. Cambridge University Press, London. 111–124.